



LEHIGH
UNIVERSITY

Library &
Technology
Services

The Preserve: Lehigh Library Digital Collections

A study for optical coherence tomography angiography of finger and phantom

Citation

Wu, Penghe, and Chao Zhou. *A Study for Optical Coherence Tomography Angiography of Finger and Phantom*. 2017, <https://preserve.lehigh.edu/lehigh-scholarship/graduate-publications-theses-dissertations/theses-dissertations/study-optical-0>.

Find more at <https://preserve.lehigh.edu/>

This document is brought to you for free and open access by Lehigh Preserve. It has been accepted for inclusion by an authorized administrator of Lehigh Preserve. For more information, please contact preserve@lehigh.edu.

A Study for Optical Coherence Tomography Angiography of Finger and Phantom

by

Penghe Wu

A Thesis

Presented to the Graduate and Research

Committee of Lehigh University

in Candidacy for the

Degree of Master of

Science

in

Bioengineering

Lehigh University

Aug 2017

Copyright
Penghe Wu

This thesis is accepted and approved in partial fulfillment of the requirements for the Master of Science.

Date

Thesis Advisor

Co-Advisor

Chairperson of Department

Table of Contents

1. Introduction	
1.1 OCT Introduction	1
1.2 OCT Angiography Introduction	5
2. Phantom Experiment	
2.1 Flow Phantom 2D Detection	9
2.2 Flow Phantom 3D Detection	13
3. OCT Imaging of Finger <i>in vivo</i>	
3.1 First Time Finger Imaging.....	15
3.2 Image Registration.....	17
3.3 Most Recent Finger Imaging.....	18
4. Conclusion	23
References	25
APPENDIX A – Image Registration Matlab Code	27
APPENDIX B – Speckle Variance Matlab Code.....	29
APPENDIX C – Complex Differential Variance Matlab Code	30
APPENDIX D – Angio-OCT Matlab Code	31
VITA.....	33

List of figures

Figure.1 A diagram of spectral domain OCT (from Ref [2])	3
Figure.2 Results of 2D flow phantom by different algorithms	11
Figure.3 SV OCT image using 4,6,8 and 10 repeated scans, respectively	12
Figure.4 CDV OCT image using 4,6,8 and 10 repeated scans, respectively	12
Figure.5 SV image with and without sub-pixel registration	13
Figure.6 MIP and a 3D rendering of 3D flowing phantom	14
Figure.7 MIP of phantom SV images with threshold from 0 to 150	15
Figure.8 Cross sectional finger structural images	16
Figure.9 Distribution of pixel shifts of a rounded tape	17
Figure.10 SV images of finger	20
Figure.11 Expected results (from Ref.[10]).	21
Figure.12 Angio-OCT images without averaging	22
Figure.13 Angio-OCT images with averaging	23
Figure.14 25 BTM-corrected Angio-OCT images	23

Abstract

The study demonstrated OCT angiography on a flowing phantom by calculating the intensity (speckle) variance between repeated frames with motion correction on a subpixel level. Other algorithms had also been tested, including phase variance, complex differential variance and Angio-OCT on both flow phantom and finger of human. The result of 3D phantom experiment and finger experiments proved that SV algorithms and Angio-OCT algorithms can be potentially used in our OCT system for finger angiography. Several different settings including scanning range, scan position density in x and y direction, number of repeated scan to use and other parameters have been tried out to improve the quality of angiographic image quality. The result of finger experiment didn't fulfill the expectation and the maximum intensity projection of angiographic image was not so clear due to the influence of motion and background noise. Some problems still remain unsolved by far. However, the experiences of data processing especially the process of frame registration lays a foundation for future research.

1. Introduction

1.1 OCT Introduction

Optical coherence tomography (OCT) is a noninvasive biomedical imaging modalities that can provide high-speed depth resolved imaging in living samples with micrometer scale resolution [1].

OCT is based on low-coherence interferometry. An OCT system has two optical arms – a sample arm, which containing the sample of interest at the end, and a reference arm, which has a mirror at the end to provide the 'reference' light. Both arms have around the same optical length. The basic principle of OCT obtaining 3D images is by measuring the echo time delay and magnitude of back-reflected light from sample at different location[2]. At first, since the first demonstration of OCT system in 1991, the mirror at the end of reference arm is moving back and forth during scanning to let 'reference' light match the light coming from different depth in sample. And this is called time domain OCT (TDOCT). However, TDOCT is no longer widely used in recent days due to its imaging speed limitation. But from physics, the depth information is stored in constructive or deconstructive light of a broadband frequency. And people can derive depth information of each A-scan in sample at once. Without moving reference arm for each A-scan, it speed ups the imaging speed dramatically. This is so called Fourier domain OCT (FDOCT). The Fourier domain OCT has two main ways of design, sweep source OCT (SSOCT) and

spectral domain OCT (SDOCT), the principle of which will be explain more detailedly later in this section. Since the main OCT system used in the thesis was SDOCT, the explanation is based on SDOCT design. In figure 1, a block diagram of spectral domain OCT is showed.

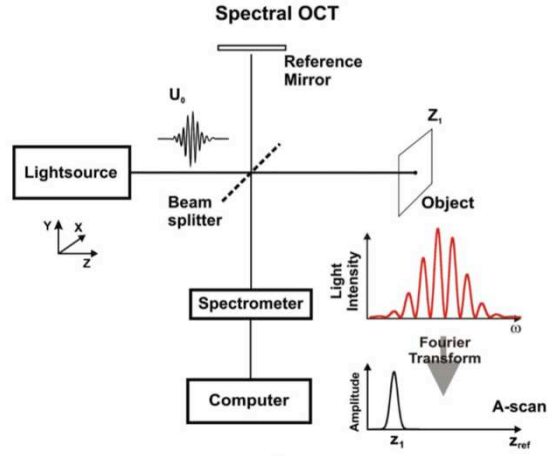


Figure 1. A diagram of spectral domain OCT (SDOCT) (From Ref [2])

The light source has a broad bandwidth that around hundreds of nanometers. It split into two optical arms by a beam splitter, and the reflected light from two arms will be coherent after beam splitter. Then the output light intensity of different wavelength can be detected by a spectrometer. Here in the paper, $S(\omega)$ is used to denote the spectrum of light source , then the output spectrum detected by spectrometer may be expressed as,

$$S_{output}(\omega) = S(\omega) \left[a_r + \sum_n a_n + 2 \sum_{m \neq n} \sqrt{a_n a_m} \cos(\tau_{nm} \omega) + 2 \sum_n \sqrt{a_r a_n} \cos(\tau_n \omega) \right] \quad (1)$$

where coefficients a_n is a series of factor characterizing back-reflected light from

measured sample. a_r is the relative reflecting factor describing the light coming from reference arm. τ_{nm} are time delays of waves returning from different layers within the examined object and do not depend on the position of the reference mirror. The first two terms represent light coming from reference arm and sample, respectively. The third term represents coherent light between different layers of the sample. The last term represents coherent light from different layers of the sample and the reference arm, which contains depth resolved information.

Then the goal becomes to solve a_n with $S_{output}(\omega)$ given. In order to reconstruct the axial structure of the measured object, an inverse Fourier transformation is applied to equation (1). Let $\Gamma(\tau)$ denotes the autocorrelation function of electromagnetic field of light $E(t)$. Then the IFT result shows below,

$$I(\tau) = (a_r + \sum_n a_n)\Gamma(\tau) + \sum_{m \neq n} \sqrt{a_n a_m} (\Gamma(\tau) \otimes \delta(\tau \pm \tau_{nm})) + \sum_n \sqrt{a_r a_n} (\Gamma(\tau) \otimes \delta(\tau \pm \tau_n)) \quad (2)$$

The last term reveals the depth resolved a_n , in other words, the relative amount of light coming from the n^{th} layer of the sample. And since the reflected light power from sample arm is relative low comparing to the power of light from reference arm. The magnitude of the third term is low and could be neglected. The first two inverse Fourier transform term can be eliminated by background subtraction.

Since applying inverse discrete Fourier transformation to a real number series will

results in a series of complex numbers. To generate structural images, we use the logarithmic scale of absolute value of complex number to represent the pixel intensity. So for structural images, the angle/phase information of complex value is unused.

Thus in SDOCT, the depth information of the sample can be obtained in each single scan. Thus, a scan system (e.g. a pair of moving mirrors to control light beam direction at the sample arm) is combined and also synchronized with camera and computer to acquire 3D structural information.

1.2 OCT Angiography Introduction

OCT can provide not only static structural information, but also provide dynamic information such as blood flow. Since OCT generates images based upon back-reflected light from the sample, the moving objects, like blood cells in vessels will tend to generate higher fluctuation of signal pattern than static region. Various OCT blood flow detection techniques have been developed for imaging vasculature structure, each of which has its own merits and drawbacks [3]. Overall there are three main types of methods, they are intensity-based methods, phase-based methods and complex value-based methods[8]. The common point in those algorithms is, to capture and quantify the signal change at the same position over a period of time, so the scanning protocol requires multiple repeated scans at the same position. Typically, with more repeated scans, the angiography images will have better

contrast and better quality. But in some cases where the sample has high movement during scanning, the ideal number of repeats may be as low as 2 or 4 to minimize the mismatch of repeats frames. Furthermore, more repeated scans means longer scanning time. In practice, this will make the patient uncomfortable or induce inevitable movement of scanning object. Generally, the optimal number of repeated scan is related to the system stability and may vary from systems and scanning protocols.

1.2.1 Intensity-Based Methods

Speckle variance (SV) is the mostly accepted algorithm in this type. The speckle variance images are generated by calculating variance of the structural pixel intensity across the number of repeated scans at the same spatial location. The equation shows as follow,

$$SV_{ijk} = \frac{1}{N} \sum_{i=1}^N [I_{ijk}(x, z) - \frac{1}{N} \sum_{i=1}^N I_{ijk}(x, z)]^2 = \frac{1}{N} \sum_{i=1}^N (I_{ijk} - I_{mean})^2 \quad (3)$$

where i, j and k are indices of frame, lateral and depth position(pixels) of the B-scan, respectively. I_{ijk} is the intensity of the pixel (j,k) in the i^{th} frame. N is the number of repeated frames (B-scans).

The reason that equation (3) can differentiate solid (static) and fluid (dynamic) regions of biological tissue is different regions have different time-dependent scattering properties [9]. For example, in the regions of non-moving region, the pixel intensities have a Gaussian distribution profile. And in flowing region of biological

tissue, such as red blood cells traveling through a vessel, where pixel intensities tend to form a Rayleigh distribution profile. And usually, as we scan same location multiple times, the intensity variance of dynamic region is higher than static region. Thus, a map that contains only moving regions (e.g. blood vessels) can be created by a simple thresholding method.

A major challenge for using SV algorithm is the effect of blood vessel shadowing artifacts [4]. The streaking and/ or shadowing artifacts encountered as one moves through the blood vessel to the deeper layers of the tissue sample can lead to an overestimation of the vascular area. To compromise the artifact, the de-shadowing process is mathematically expressed as,

$$SVDS_{ijk} = SV_{ijk} \times e^{\frac{1}{\gamma} \sum_{z=1}^{k-1} SVDS(i,j,z)} \quad (4)$$

where γ is a constant to control the rate of attenuation. In this de-shadowing process, the SV signal is attenuated by a factor from the top surface of the tissue.

There are also other intensity-based algorithms that use equations other than equation (3), one example is Eq.(1) from ref.[10]:

$$OCTAngio_{i,j,k} = \frac{\sum_{j=1}^J \sum_{k=1}^K (I_{i,j,k} - I_{i+1,j,k})^2}{\sum_{j=1}^J \sum_{k=1}^K (I_{i,j,k}^2 + I_{i+1,j,k}^2)} \quad (5)$$

where $I_{i,j,k}$ is the amplitude of the OCT image and i, j, and k are indices for the frame, transverse, and depth pixels, respectively. K is the number of averaged depth pixels and J is the number of averaged A-lines (lateral direction).

1.2.2 Complex value-based Variance

The complex value-based methods include optical microangiography (OMAG) [6] and the complex differential variance (CDV) approach [5]. Those algorithms use both intensity and phase information from OCT signal. The equation of CDV algorithm shows as below,

$$f_{CDV}(z) = \sqrt{1 - \frac{\sum_{t=1}^{M-1} \left| \sum_{k=-L}^L w(k) R(z-k, t) R^*(z-k, t+1) \right|}{\sum_{t=1}^{M-1} \sum_{k=-L}^L w(k) \frac{1}{2} \left[|R(z-k, t)|^2 + |R(z-k, t+1)|^2 \right]}}, \quad (6)$$

where the complex OCT signal is expressed as $R(z, t) = A(z, t)e^{i\phi(z, t)}$, M is the number of repeated B-scan at the same location, w(k) is a depth window function of length 2L+1. The algorithm calculates the ratio of the summation of magnitude of a complex correlation term between adjacent time points across the depth kernel to a similar summation of magnitudes.

1.2.3 Phase Variance (PV)

Similar to speckle variance algorithm, phase variance algorithm are generated by focusing on the phase variance of the of OCT signal across repeated scans at the same spatial location.

There are other similar algorithms that calculating the variance of intensity or phase difference two adjacent frames within repeated frames. And other algorithms include Doppler-based or histogram-based algorithm. But since I have not implement other algorithms, the knowledge of those is limited and they are not introduced here.

2. Phantom Experiments

The OCT system used for angiography study utilizes a superluminescent laser as light source, which has the central wavelength of 1320 nm and bandwidth of 110 nm that provides a 6.3 μm axial resolution in the air. The transverse resolution is about 8 μm when putting a 5X objective at the sample arm (~ 6 μm with 10X objective). And the A-scan speed was 20.7kHz or 47kHz or 92kHz depending on situation.

2.1 flow phantom 2D detection

In order to optimize scanning protocol, to find out the number of repeated B-scans are necessarily enough and what spacing between the scan positions will give the best image quality, at first, a series of flow phantom experiments were performed.

The flow phantom is made of a soft plastic tube filled with diluted milk, and covered with a mixture of gel and jelly as non-moving contrast region. The tube was connected to a syringe and an infusing pump, so the diluted milk was flowing inside the tube at a constant speed. The outer diameter of the tube was around ~ 0.8 mm and

the inner diameter was ~ 0.4 mm. The liquid average flowing speed inside the tube was calculated as ~ 16 mm/s. For reference, the blood flow speed in human capillaries is ~ 0.3 mm/s and ~ 400 mm/s in aorta. So to be honest, the flow phantom cannot fully simulate the human tissue environment due to its relative high flowing speed and large diameter. The phantom as a whole was not moving and was able to help to find out a good scanning protocol and test the stability of the system, also provide a comparison between different angiography algorithms. (Before this 2D flow phantom experiment, a similar 3D Brownian motion phantom experiment was performed, the phantom was filled the tube with chocolate milk but without pump, but this 2D flow phantom gave a better result.)

The A-scan speed for 2D phantom experiment was set to be at 20.7 kHz. The scanning range for above experiments was set to 2 mm for x direction and 0 for y direction. A-scan number per B-scan varies from 100 to 800 (higher A-scan number per B-scan means better image quality but longer scanning time). Either 200 repeated B-scans or 100 repeated B-scans were used, which both were high enough for I plan to achieve.

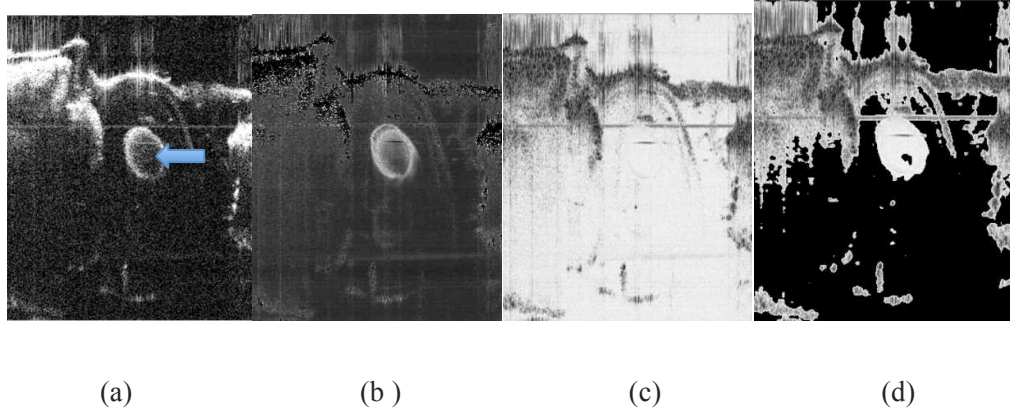


Figure 2. 2D flow phantom (a) one frame of phantom structural OCT image with 300 positions in x range. The blue arrow indicates the diluted milk flowing inside the tube. Other bright structures were either tube outer surface or the gel that was non-moving (b) Speckle variance (SV) OCT image using 200 repeated B-scans. (c) Complex differential variance (CDV) OCT image using 200 repeated B-scans. (d) CDV OCT image after applied a background mask from structural image.

From above figures, it shows that SV algorithm can differentiate non-moving part and the flowing part in these settings. CDV algorithm is able to differentiate the non-moving part from moving part and background, but failed to differentiate background and flowing part itself. But when apply the background mask generated from structural image, and a simple thresholding method can make only the flowing part show up.

However, in real case, it is impossible to use such high number of repeated scans. Next, only a certain number of successive frames (4, 6, 8, 10) was used. The result shows in Figure.3.

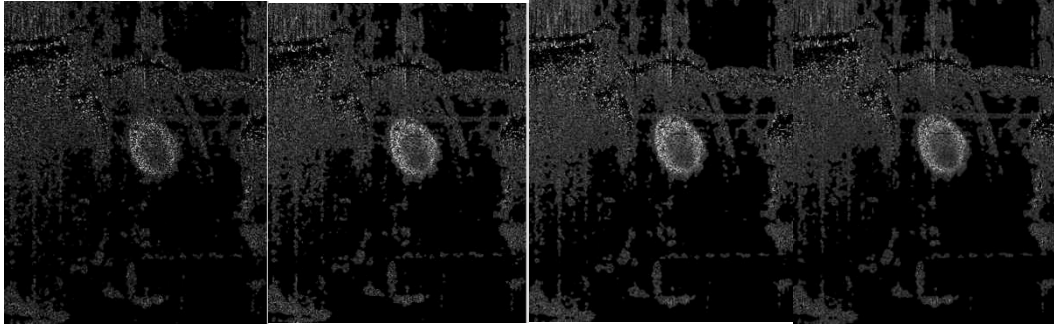


Figure 3. SV OCT image using 4,6,8 and 10 repeated scans, respectively

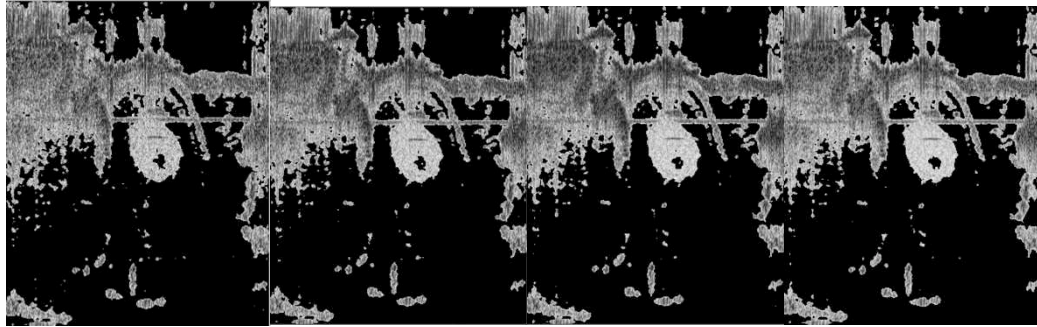


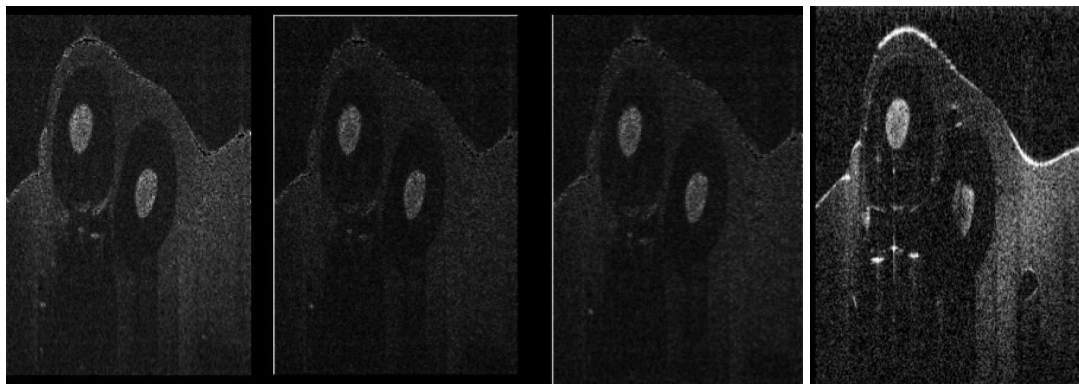
Figure 4. CDV OCT image using 4,6,8 and 10 repeated scans, respectively

The image quality is increased with number of repeated frames used. A compromise can be made between total scanning time and image quality based on this. In next experiment, at least 6 repeated scans per position was preferable.

Besides, the phase variance (PV) algorithm was not working for the system or at least for the 2D and 3D phantom datasets acquired. So the PV OCT images are not showing here and after.

2.2 flow phantom 3D detection

In 3D flow phantom experiment, the camera line rate (A-scan speed) was increased to 47kHz from 20.7kHz to reduce scanning time. Then the frame rate increased from 69 frames/sec to 157 frames/sec. And as before, scan protocol has 300 by 300 positions with 8 repeated B-scans covering a 2mm by 2mm area. The phantom was a tube node with diluted milk flowing inside covered by gal. This time, in order to correct motion influences, I came up with a new data process flow path. From registration check, I found most shifts are within single pixel level. So I first enlarge original structural images, to increase the image size 5 times, and then perform registration and SV after. At last, the enlarged processed image will be resize back. I call it sub-pixel registration. The result looks promising.



(a)

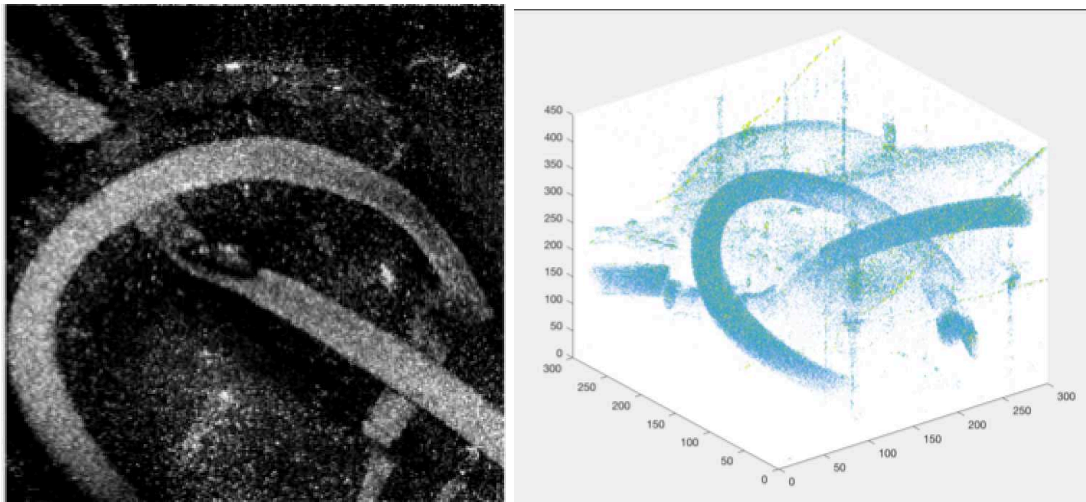
(b)

(c)

(d)

Figure.5 (a) SV image without sub-pixel registration (b) SV image with 5 times sub-pixel registration (c) SV image with 5 times sub-pixel registration (d) corresponding structural frame at same position

Comparing between a, b and c, we know this new method works well that can enhance the contrast between moving region and static region. And enlarging original image by 20 times gives the nearly same result as enlarging 5 times in this case. And after setting a proper threshold, SV images will be left with flowing part mostly. The result shows in Figure 6. And Figure 7 shows the results with different threshold from 0 to 150.



(a)

(b)

Figure.6 (a) An *en face* maximum intensity projection (MIP) of SV images (b) A 3D rendering of flowing region. The node structure is clear

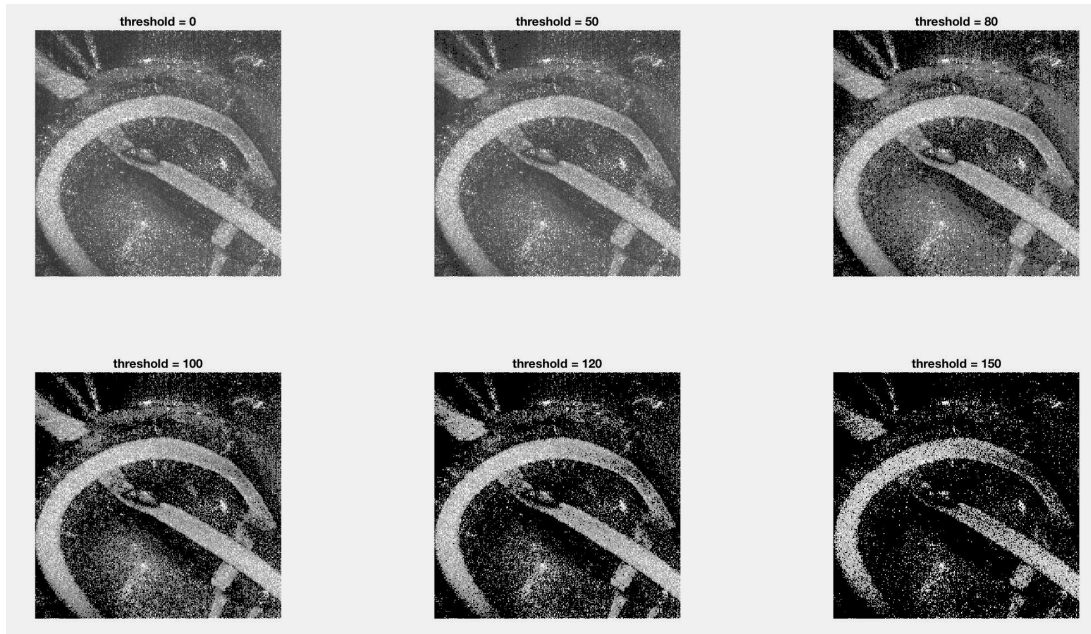
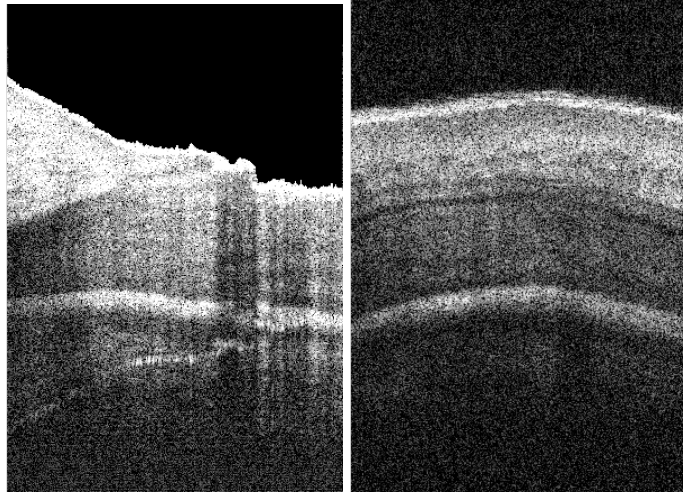


Figure.7 MIP of phantom SV images with threshold from 0 to 150

3. OCT imaging of finger *in vivo*

3.1 First time finger imaging

Then several datasets were taken using my own index finger. The region that focused on was the conjunction between nail and finger, the structural images are as shown below:



(a)

(b)

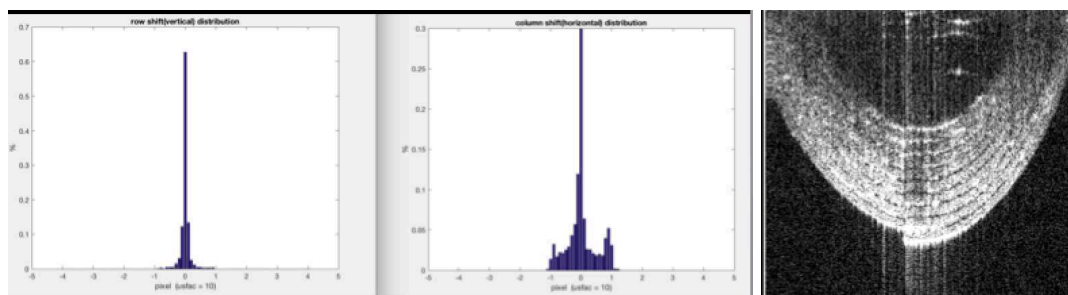
Figure 8. Cross sectional finger structural images, (a) as finger pointing along fast axis (b) as finger pointing along slow axis

The imaging range was 2 mm by 2mm with 300 by 300 scan positions. The number of repeated frame used for above case was 8. However, due to the movement of finger during scanning when the finger is freely placed on the stage, it's hard to tell the *en face* projection result this time could show clear capillary structures. I was still not sure it was because the algorithm not working or due to finger movement during scanning. So before performing another finger experiment, I decided to study image registration a little bit and try to minimize influences of the bulk tissue motion.

3.2 Image registration

The image registration code I used in the thesis was written by in Manuel and Guizar in Matlab [11]. It calculates the cross correlation between two frames, and then refine column and row shift based on the cross correlation peak. It can also make shift estimation with up-sampling that can provide shift estimation at sup-pixel level. After some tests, evidences shows that the code can work accurately for the measurement. The advantage of this algorithm is its fast speed and small memory occupation.

Before testing image registration with a flow phantom, its necessary to check how much is that pixel shift in vertical and horizontal direction in a static situation, and then tried to find causes to explain. A rounded tape was used with same scanning protocol as finger study. The column and row shifts distribution (upsampling factor 10) shown as below:



(a)

(b)

(c)

Figure.9 (a) row shift (vertical direction) distribution (b) column shift (horizontal direction) distribution (c) A cross sectional structural frame

The vertical direction has nearly no shift and horizontal direction has mostly shift within one pixel. At static situation, there are several possible reasons to cause this distribution pattern. First, the physical vibration of the stage is inevitable and mostly reflected in vertical direction. In horizontal direction, this is minor cause compare to others. Second, the imperfect synchronization between camera (computer) and scanning mirror. A low DAC updating rate is one possible reason. The DAC updating rate is the sampling rate for voltage sending from computer to control scanning mirrors. However, as the DAC updating rate increased from 40k samples per second to 1 million samples per second, the horizontal shift did not decrease. An oscilloscope was directly connected to scanning control system to measure the voltage sending from computer. I suspect the noise might be one key reason, but I didn't investigate further when registration and SV algorithm worked well for a 3D phantom experiment.

3.3 Most recent finger imaging

The system noise and bulk tissue motion are inevitable during scanning, and from previous experiences, these two key factors that influence the angiography result. Besides, the speed of blood flow in microvascular within finger is much lower than the speed of diluted milk in phantom experiment. In other papers of OCT finger

angiography imaging, the camera speed is similar [6][10], or higher [7][12] than the camera speed, which is 47kHz, used in previous finger and phantom experiment. And after calculating, the frame rate is either close or half as their settings. So, the frame rate may not be sufficient to visualize the slow blood flow inside microvascular within the finger. And according to ref. [12], a small gate length (number of repeated scan) of either 2 or 4 and a fast frame rate are desired to obtain a high SV signal-to-noise ratio (SNR). So, in this experiment, the camera speed was increased to 92kHz and number of A-scan per B-scan reduced from 300 to 200, the scanning range increased from 2 by 2 mm to 4.5 by 4.5 mm to adjust A-scan density close to the settings in above references. Thus, the frame rate increased from 157 frames/sec to 390 frames/sec. Along slow axis, for each position, there were 6 repeated Bscans. The gatelength chose for post-processing includes 2,4 and 6. I also acquired data with unchanged camera speed, which is 47kHz, however, none of them shows improving result. Here in the paper, only images with 92kHz camera speed will be showed.

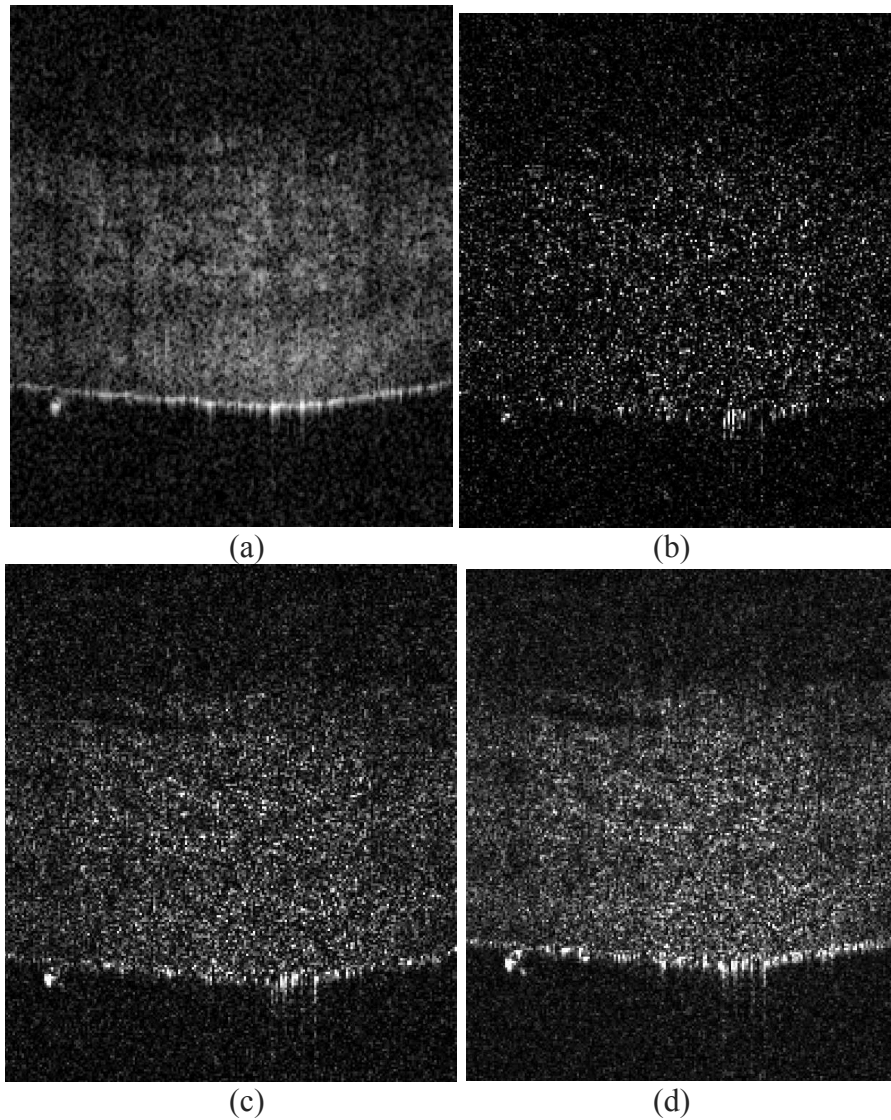


Figure.10 A frame of (a) Structural image of finger (b)(c)(d) corresponding SV image with gatelength 2,4 and 6

In the image, the surface is at the bottom. This reason I put this way is because it can increase SNR in deep region. The SV images didn't show any vascular structure beneath the finger surface. The surface boundary is bright, and that is due to the strong reflection at the surface, not because of the imperfectness in registration. And the brightness at the surface will not influence the result. The registration process

was directly after raw structural images generated, at each position, the code would shift the rest of 5 frames to the first frame. After careful registration with upsampling factor of 10, each SV frame or each pixel was calculated using equation (3). However, in the SV image showing above, there is no difference between flowing region and static tissue in terms of pixel intensity. The expected results show in Figure.11, from ref [10]. After, combing angiography frames to make a 3D rendering or a MIP projection to reveal the vascular structure.

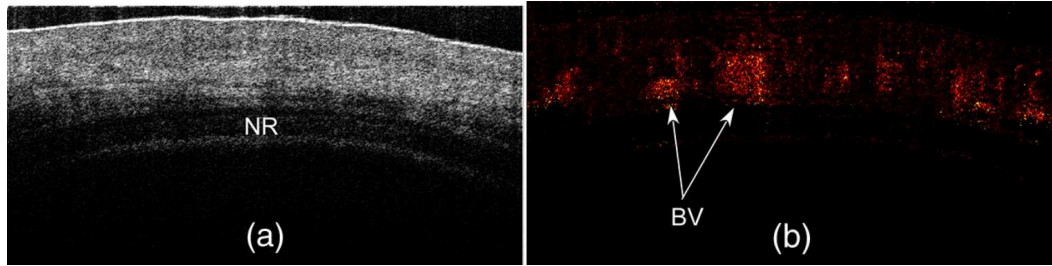


Figure.11 Expected results. Two pictures are from Ref.[10]. (a) An OCT image of a human finger nail-fold region. (b) OCT angiography image of that frame.

For the same dataset, another intensity-based angiography method was performed using equation (5). And equation (5) only works on two repeated frames (gatelength equals to 2), a slight change was made, as below, to ensure it can apply to higher gatelength, and still remain consistent to original when gatelength equals 2.

$$OCTAngio_{i,j,k} = \frac{\sum_{j=1}^J \sum_{k=1}^K N \times var(I_{j,k})}{\sum_{j=1}^J \sum_{k=1}^K \sum_i I_{j,k}^2} \quad (7)$$

where N is the gatelength (number of repeated frames used), $var(I_{j,k})$ is the variance of the pixel over gatelength of frames. For J=1, K=1, when no averaging was taken,

the angiography result shows in Figure.12. The processed image was cropped to remove up and down background.

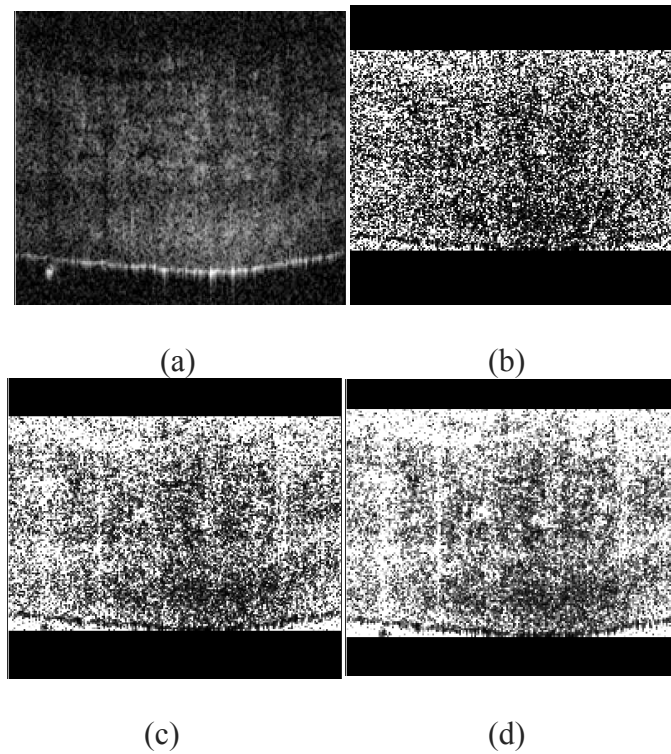


Figure.12 (a) cross sectional structural image of finger (b)(c)(d) corresponding processed image with gatelength 2,4 and 6 using Eq.(7) where $J=K=1$

It's not working. The difference between Eq.(3) and Eq.(7) is, for each pixel in Eq(7), the variance value is divided by the summation of squared intensity. This kind of 'normalization' leads to a complementary-like image of original averaged structural image. I also tried to normalization by dividing the square root of the summation at bottom, however, it will only results in nearly homogeneously distributed snowlike images.

For $J=3$, $K=3$, after averaging over 3 by 3 pixels, the noise level got reduced and the contrast of different area start to look clear. However, the problem remains still that the dark area in structural image transfer to bright area in processed image and vice versa.

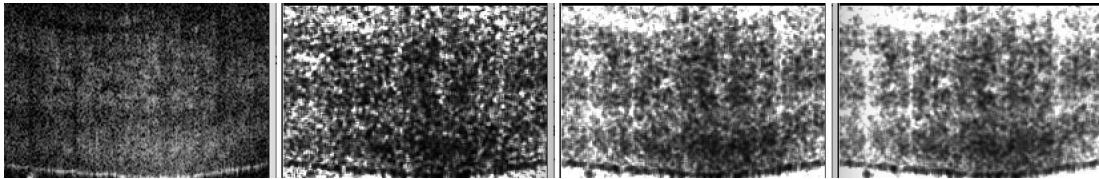


Figure.13 a cross sectional structural image of finger with its corresponding processed image with gatelength 2,4 and 6 using Eq.(7) where $J=K=3$

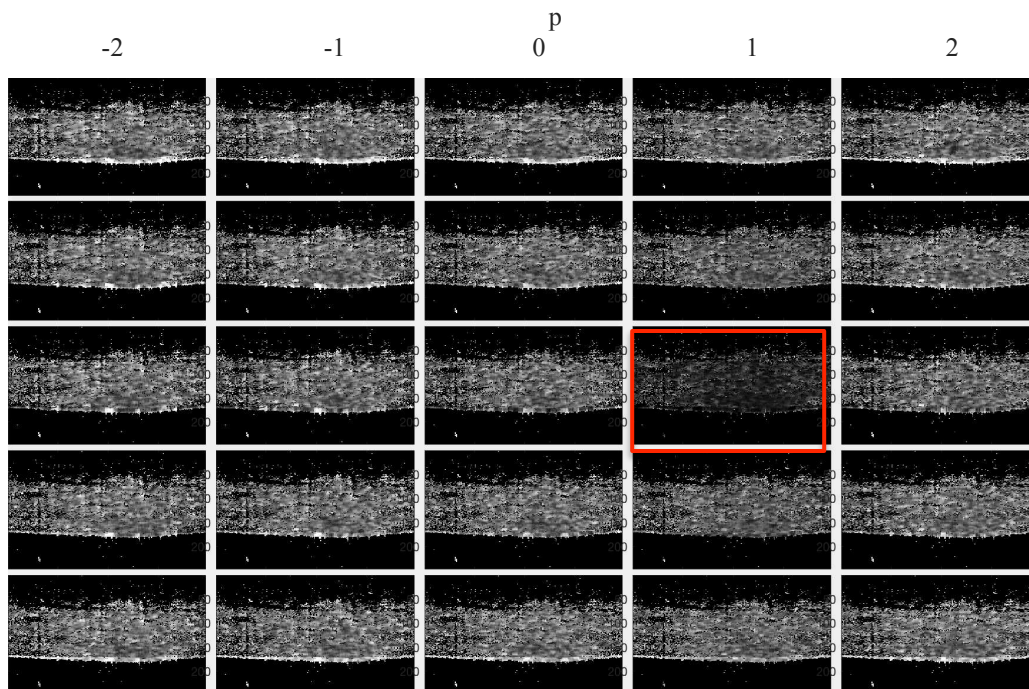


Figure.14 Processed 25 OCT angiographic images for BTM correction. Solid red square indicates .
BTM-corrected OCT angiography.

4. Conclusion

The study demonstrated OCT angiography on a flowing phantom by calculating the intensity (speckle) variance between repeated frames with motion correction on a subpixel level. Other algorithms had also been tested, including phase variance, complex differential variance and Angio-OCT (normalized squared difference between repeated frames, a method based on Ref. [12]) on both flow phantom and human finger. The result of 3D phantom experiment proved that SV algorithms can be potentially used in our OCT system for finger angiography. Several different settings in terms of scanning range, scan position densities, gatelength (number of repeated scan) have been tried out. However, the result of finger experiment didn't meet the expectation due to two main reasons. First, the untied finger had much more motion than sitting-on phantom during scanning. Even though the imaging registration code can align the repeated frames. The position of repeated frames that supposed to be at the same position may be different. The registration code cannot help with the motion in y direction. Using lower gatelength and increasing camera speed may reduce the influence of motion, but it trades off the image quality and also increases the noise level. Second, the noise of background is an unsolved problem. In finger and even in phantom results, not any algorithms including PV, CDV and Angio-OCT could give a low intensity value at background region.

References

1. Drexler, Wolfgang, et al. "Optical coherence tomography today: speed, contrast, and multimodality." *Journal of biomedical optics* 19.7 (2014): 071412-071412.
2. Wojtkowski, Maciej. "High-speed optical coherence tomography: basics and applications." *Applied Optics* 49.16 (2010): D30-D61.
3. Mahmud, Mohammad Sultan, et al. "Review of speckle and phase variance optical coherence tomography to visualize microvascular networks." *Journal of biomedical optics* 18.5 (2013): 050901-050901.
4. Yang, Victor XD, et al. "Improved phase-resolved optical Doppler tomography using the Kasai velocity estimator and histogram segmentation." *Optics Communications* 208.4 (2002): 209-214.
5. Nam, Ahhyun S., Isabel Chico-Calero, and Benjamin J. Vakoc. "Complex differential variance algorithm for optical coherence tomography angiography." *Biomedical optics express* 5.11 (2014): 3822-3832.
6. An, Lin, Jia Qin, and Ruikang K. Wang. "Ultrahigh sensitive optical microangiography for in vivo imaging of microcirculations within human skin tissue beds." *Optics express* 18.8 (2010): 8220-8228.
7. Xu, Jingjiang, et al. "Scalable wide-field optical coherence tomography-based angiography for in vivo imaging applications." *Biomedical optics express* 7.5 (2016): 1905-1919.

8. Baran, Utku, and Ruikang K. Wang. "Review of optical coherence tomography based angiography in neuroscience." *Neurophotonics* 3.1 (2016): 010902-010902.
9. Cheng, Yuxuan, et al. "Statistical analysis of motion contrast in optical coherence tomography angiography." *Journal of biomedical optics* 20.11 (2015): 116004-116004.
10. Watanabe, Yuuki, Yuhei Takahashi, and Hiroshi Numazawa. "Graphics processing unit accelerated intensity-based optical coherence tomography angiography using differential frames with real-time motion correction." *Journal of biomedical optics* 19.2 (2014): 021105-021105.
11. Guizar-Sicairos, Manuel, Samuel T. Thurman, and James R. Fienup. "Efficient subpixel image registration algorithms." *Optics letters* 33.2 (2008): 156-158.
12. Lee, Kenneth KC, et al. "Real-time speckle variance swept-source optical coherence tomography using a graphics processing unit." *Biomedical optics express* 3.7 (2012): 1557-1564.
13. Wang, Ruikang K., et al. "Three dimensional optical angiography." *Optics express* 15.7 (2007): 4083-4097.
14. Wang, Ruikang K., and Lin An. "Doppler optical micro-angiography for volumetric imaging of vascular perfusion in vivo." *Optics express* 17.11 (2009): 8926-8940.
15. Liu, Gangjun, et al. "High-resolution imaging of microvasculature in human skin in-vivo with optical coherence tomography." *Optics express* 20.7 (2012): 7694-7705.
16. Ruminski, Daniel, et al. "OCT angiography by absolute intensity difference applied to normal and diseased human retinas." *Biomedical optics express* 6.8 (2015): 2738-2754.
17. Zhang, Anqi, et al. "Methods and algorithms for optical coherence tomography-based angiography: a review and comparison." *Journal of biomedical optics* 20.10 (2015): 100901-100901.
18. Lee, Hsiang-Chieh, et al. "Circumferential optical coherence tomography angiography imaging of the swine esophagus using a micromotor balloon catheter." *Biomedical Optics Express* 7.8 (2016): 2927-2942.
19. Zhang, Miao, et al. "Projection-resolved optical coherence tomographic angiography." *Biomedical optics express* 7.3 (2016): 816-828.

20. Wang, Ruikang K., et al. "Wide-field optical coherence tomography angiography enabled by two repeated measurements of B-scans." *Optics letters* 41.10 (2016): 2330-2333.
21. Motaghiannezam, Reza, and Scott Fraser. "Logarithmic intensity and speckle-based motion contrast methods for human retinal vasculature visualization using swept source optical coherence tomography." *Biomedical optics express* 3.3 (2012): 503-521.
22. Yousefi, Siavash, Zhongwei Zhi, and Ruikang K. Wang. "Eigendecomposition-based clutter filtering technique for optical microangiography." *IEEE Transactions on Biomedical Engineering* 58.8 (2011): 2316-2323.

Appendix A

Image registration

```
clear;
close all;
tic;
%% read images
foldername='/Users/wupenghe/Desktop/Angiography/phantoms/finger3/92kHz/';
NumBScan = 900;
Repeatframe = 6;
gatelength = Repeatframe;
filename = strcat(foldername, 'finger3_92.tiff');

for j=1:NumBScan
    img1=imread(filename,j);
    volume_log(:,j)=double(img1);
end
Zpix = size(volume_log,1);
numAscansPerBscan = size(volume_log,2);

%% bg process
% mask = zeros(Zpix,numAscansPerBscan,NumBScan/gatelength);
% h_filter = fspecial('gaussian',5,1);
% noise_mean = 28;
% for i=1:NumBScan/gatelength
%     mask(:,i) = mean(volume_log(:,1+(i-1)*gatelength:i*gatelength),3);
%     mask(:,i) = imfilter(mask(:,i),h_filter);
% end
% mask(mask <= noise_mean) = 0;
% mask(mask > noise_mean) = 1;
% savepathopen=[foldername 'bgmask/'];
```

```

% mkdir(savepathopen);
% %imwrite(mask(:, :, 1), [savepathopen 'bgmask.tiff'], 'WriteMode', 'overwrite');
% delete([savepathopen 'bgmask.tiff']);
% for frameNum=1:NumBScan/gatelength
%   imwrite(mask(:, :, frameNum), [savepathopen 'bgmask.tiff'], 'WriteMode', 'append',
'Compression','none');
%   %imwrite(mask(:, :, frameNum),[savepathopen num2str(frameNum) '.tiff'], 'tif');
% end

%%% dft registration
usfac = 10;
volume_regis = zeros(size(volume_log));
IdxShift = zeros(2,NumBScan);
%Shift = zeros(2,NumBScan);
for framegroup=1:NumBScan/Repeatframe
    frame1 = volume_log(:, :, (framegroup-1)*Repeatframe+1);
    for num = 1:Repeatframe
        frameNum = (framegroup-1) * Repeatframe + num;
        frame2 = volume_log(:, :, frameNum);
        a = dfregistration(fft2(frame1),fft2(frame2),usfac);
        IdxShift(1,frameNum) = a(3);
        IdxShift(2,frameNum) = a(4);
        %Shift(:,frameNum) = [fix(IdxShift(3)); fix(IdxShift(4))];
        frame = imresize(volume_log(:, :, frameNum),usfac);
        frame = circshift(frame,round([IdxShift(1,frameNum)*usfac IdxShift(2,frameNum)*usfac]));
        volume_regis(:, :, frameNum) = imresize(frame,1/usfac);
    end
    % framegroup
end
% save([foldername 'Shift.mat'],'Shift','-v7.3');

%%% save pic after registration
savepath=[foldername];
mkdir(savepath);
image_regis = uint8(volume_regis);
delete([savepath 'regis.tiff']);
disp('registration finished');
for frameNum=1:NumBScan
    imwrite(image_regis(:, :, frameNum), [savepath 'regis.tiff'], 'WriteMode', 'append',
'Compression','none');
    %imwrite(mask(:, :, frameNum),[savepathopen num2str(frameNum) '.tiff'], 'tif');
end
toc;

```

Appendix B

Speckle variance OCT

```
clear all;
close all;
tic;
%% Setups
foldername='/Users/Desktop/Angiography/phantoms/finger3/92khz/';
NumBScan = 720;
Repeatframe = 6;
Repeatframe_use = 6;
gatelength = Repeatframe_use;
filename=strcat(foldername, 'regis.tiff');
%% read regis data
for j=1:NumBScan
    img1=imread(filename,j);
    volume_log(:,j)=double(img1);
end
Zpix = size(volume_log,1);
numAscansPerBscan = size(volume_log,2);

%% svOCT - Review of speckle and phase variance optical coherence tomography to visualize
microvascular networks
sv_volume = zeros(Zpix,numAscansPerBscan,NumBScan/Repeatframe);
factor = 1;
for i = 1:NumBScan/Repeatframe
    sv_volume(:,i) = factor .* var(volume_log(:,:(i-1)*Repeatframe+1):((i-1)*Repeatframe+gatelength)),1,3);
end
%% save
Imax = mean(max(max(sv_volume)));
```

```

factor = 500./Imax; %since the noise or some pixels have extreme high intensity(255), using factor
higher than 255 will saturate those pixels and can increase the contrast
sv_volume = sv_volume .* factor;
sv_volume_int = uint8(sv_volume);
savepathopen=[foldername 'svOCT_g6/'];
mkdir(savepathopen);
delete([savepathopen 'svOCT.tiff']);
for frameNum=1:size(sv_volume,3)
    imwrite(sv_volume_int(:, :, frameNum), [savepathopen 'svOCT.tiff'], 'WriteMode', 'append',
'Compression','none');
end
% deshadowing process
% volume_deshadowing=exp(-cumsum(volume_sv,1)/3e2);
% volume_sv_fi=volume_sv.*volume_deshadowing;
%
volume_sv=squeeze(mean(reshape(volume_final(:,1:floor(numAscansPerBscan/Mframe)*Mframe,:),t
otalx,Mframe,floor(numAscansPerBscan/Mframe),NumBscan),2));
% volume_sv_fi=log(volume_sv_fi);

```

Appendix C

Complex differential variance OCT

```

clear;
close all;
tic;
foldername = '/Users/wupenghe/Desktop/Angiography/phantoms/3D/';
path_cplx = [foldername 'VolumeCplx.mat'];
tt=['load ' path_cplx ' volume_cplx;'];
eval(tt);
%% settings
Repeatframe = 8;
gatelength = Repeatframe;
Zpix = size(volume_cplx,1);
numAscansPerBscan = size(volume_cplx,2);
NumBScan = size(volume_cplx,3);
%% CDV
cdv_volume = zeros(Zpix,numAscansPerBscan,NumBscan/gatelength); %complex differential
variance
L = 2;
depth_win = ones(1,2*L+1);
%depth_win = fspecial('gaussian',[1 2*L+1],0.8);
volume_cplx2 = zeros(Zpix+2*L , numAscansPerBscan , NumBScan);
for i = 1:NumBScan
    volume_cplx2(L+1:Zpix+L, :, i) = volume_cplx(:, :, i); %pad volume_cplx with 0 at top and bottom
end
for i = 1:NumBScan/gatelength
    sum_top = zeros(Zpix,numAscansPerBscan);
    sum_bot = zeros(Zpix,numAscansPerBscan);
    for j = 1:gatelength-1
        buffer = zeros(Zpix,numAscansPerBscan);
        for k = 1:2*L+1

```

```

        buffer = buffer + depth_win(k) * volume_cplx2(k:k+Zpix- 1,:(i-1)*gatelength+j) .*
        conj(volume_cplx2(k:k+Zpix-1,:(i-1)*gatelength+j+1));
        sum_bot = sum_bot + (1/2) * depth_win(k) * (abs(volume_cplx2(k:k+Zpix-1,:(i-
1)*gatelength+j)).^2 + abs(volume_cplx2(k:k+Zpix-1,:(i-1)*gatelength+j+1)).^2);
        end
        sum_top = sum_top + abs(buffer);
        end
        cdv_volume(:,i) = sqrt(1-sum_top./sum_bot);
    end
    for i = 1 : NumBScan/gatelength
        mask(:,i) = imread([foldername 'bgmask/bgmask.tiff'],i);
    end
    mask = double(mask);
    cdv_volume = cdv_volume .* (mask/255);
    %% save
    ...

```

```
toc;
```

Appendix D

Angio-OCT

```

clear all;
close all
tic;
%% Setups
foldername='/Users/wupenghe/Desktop/Angiography/phantoms/finger3/92khz/';
NumBScan = 720;
Repeatframe = 6;
Repeatframe_use = 4;
gatelength = Repeatframe_use;
filename=strcat(foldername, 'regis.tiff');
%% read regis data
for j=1:NumBScan
    img1=imread(filename,j);
    volume_log(:,j)=double(img1);
end
Zpix = size(volume_log,1);
numAscansPerBscan = size(volume_log,2);

%% Angio-OCT - Graphics processing unit accelerated intensity-based optical coherence tomography
angiography using differential frames with real-time motion correction

% plus averaging
m = 3; %# of pixels in lateral direction to average
n = 3; %# of pixels in depth direction to average

angio_volume = zeros(Zpix-n+1,numAscansPerBscan-m+1,NumBScan/Repeatframe);
for i = 1:NumBScan/Repeatframe
    a1 = gatelength * var(volume_log(:,:(i-1)*Repeatframe+1):(i-1)*Repeatframe+gatelength),1,3);
    a2 = zeros(Zpix,numAscansPerBscan);

```

```

for j = 1:gatelength
    a2 = a2 + volume_log(:,:,i-1)*Repeatframe+j).^ 2;
end
% a2 = sqrt(a2);
b1 = zeros(Zpix,numAscansPerBscan);
b2 = zeros(Zpix,numAscansPerBscan);
for jj = 0:m-1
    for kk = 0:n-1
        b1 = b1 + circshift(a1,[-kk -jj]);
        b2 = b2 + circshift(a2,[-kk -jj]);
    end
end
angio_volume(:,:,i) = b1(1:end-n+1,1:end-m+1) ./ b2(1:end-n+1,1:end-m+1);
end
angio_volume(isnan(angio_volume)) = 0;

%% mask creation
%%for inverse picture position (surface at bottom)
mask = zeros(Zpix,numAscansPerBscan,NumBScan/Repeatframe);
h = 128;
for i = 1:NumBScan/Repeatframe
    h2 = round(-100/119*i+28660/119); % for finger3_47_2
    h1 = h2 - h;
    if h1 < 0
        h1 = 0;
    end
    mask(h1:h2,:,i) = 1;
end

%% for normal picture position (surface at top)
% mask = zeros(Zpix,numAscansPerBscan,NumBScan/Repeatframe);
% h = 150;
% for i = 1:NumBScan/Repeatframe
%     h1 = round(2/3*i+49); % for finger3_47_2
%     h1 = round(95/119*i+2880/119); % for finger3_47_1
%     h2 = h1 + h;
%     if h2 > Zpix
%         h2 = Zpix;
%     end
%     mask(h1:h2,:,i) = 1;
% end
angio_volume = angio_volume .* mask(1:Zpix-n+1,1:numAscansPerBscan-m+1,:);

%% save
...

toc;

```

VITA

Name: Penghe Wu

Date of birth: July 31, 1992

Education:

2011 – 2015	Tsinghua University, China	B.S
	Major: Engineering physics	
2015 – 2017	Lehigh University, USA	M.S (expected)
	Major: Bioengineering	